Communication

Two-Dimensional Beam Steering Based on Compact Programmable Coding Metasurface

Fei Yang *, Fan Xu, Chenxi Liu (ID)**, Xinyu Yang, Ziqiang Wang, Junwei Wu and Xiaojian Fu**

State Key Laboratory of Millimeter Waves, Southeast University, Nanjing 210096, China
* Correspondence: yangfei@seu.edu.cn

Featured Application: The proposed metasurface in the article can be used in millimeter wave sensing and 5G wireless communications.

Abstract: A programmable coding metasurface provides unprecedented flexibility to manipulate electromagnetic waves dynamically. By controlling the peculiarity of subwavelength artificial atoms, devices with metasurfaces perform various functionalities. In this paper, a compact programmable coding metasurface with PIN diodes is proposed to realize the beam steering in the Ka band. The phase distribution on the metasurface can be actively controlled by switching the states of each meta-atom. By tuning the phase gradient along the metasurface plane, the reflective beam can scan all directions in the upper half-plane. In addition, the compact metasurface is easier to integrate, which could expand the fields of applications. The full-wave simulation results show that the radiation direction of the main lobe is consistent with the theoretical calculation results, and the maximum steering angle of simulation is 60°. As experimental verification, a prototype was processed and the functionality of beam steering in the xoz plane and in the yoz plane was tested. Experimental results show that the designed metasurface can achieve beam steering in both planes, and the maximum scan angle is 45° in the xoz plane. The proposed metasurface opens a new way of beam steering in half space, which may have potential applications in sensing and wireless communications in millimeter waves.

Keywords: programmable metasurface; digital coding metasurface; phase shifter; beam steering; millimeter wave; compact metasurface

1. Introduction

Metasurfaces, as a two-dimensional form of metamaterial, have gained considerable interest for their high flexibility and accuracy in the manipulation of electromagnetic (EM) waves [1–3]. Inspired by the generalized Snell's law, metasurfaces with phase discontinuities imparted can be used to manipulate the wavefront, and the anomalous reflection and refraction can be observed [4–6]. In the past decade, many passive metasurfaces have been designed, fabricated, and implemented in many applications, such as polarization conversions, beam forming, optical focus, and holograms [7–11]. Although these passive metasurfaces offer extremely strong EM manipulation capabilities, real-time control of EM waves has been in high demand for many practical applications such as high-speed communications, remote sensing, imaging, and radar [12–14].

In the past decade, the concept of digital coding and programmable metasurfaces was proposed and developed, which bridges the physical and digital worlds [15,16]. By encoding different states of the meta-atoms, the function of a metasurface can be represented by a string of binary codes [17]. Furthermore, these binary codes bring us an information science perspective on metasurfaces, and provide a new wireless communication architecture [18,19]. For the 1-bit digital coding metasurface, two states with a 180° phase difference are required, and the two states can be encoded as digital codes "0" and

"1," respectively. By changing the digital coding sequence, the phase distribution of the metasurface is changed, and the function of the metasurface is also determined. To date, digital metasurfaces have extensively achieved different functions, such as beam steering, orbital angular momentum (OAM) beams, holograms, and so on [10,20,21].

In this paper, a 1-bit programmable reflective metasurface is designed, fabricated, and tested. The metasurface can realize two-dimensional dynamic beam steering with loaded PIN diodes. The millimeter wave metasurface possesses 16×16 meta-atoms using the double-patch metal pattern. With the careful design of the digital control system and the biasing network, the phase of the 256 meta-atoms can be modulated independently. Simulation results show that the metasurface can achieve flexible two-dimensional beam steering in the upper half-plane with a maximum steering angle of $60°$. In addition, the compact metasurface is only 6.4 cm $\times$ 6.4 cm in size. For experimental verification, we processed a prototype and tested it in a standard microwave anechoic chamber. Experimental results show that the designed metasurface can achieve a maximum steering angle of $45°$ in the upper half-plane. Programmable metasurfaces which combine the performance of arrays and aperture antennas can provide an efficient and low-cost platform for high-gain adaptive beam steering. The proposed metasurface with its excellent beam-steering capability has great application in many fields such as radar, communication, and remote sensing.

2. Design and Simulation

The profile of the programmable coding metasurface is shown in Figure 1. It consists of 16 rows and 16 columns of meta-atoms, and each atom contains three layers of metal and two layers of dielectric. The structure of each atom is demonstrated in Figure 2: there are two rectangular metal patches on the top metal layer, and a PIN diode is loaded between the two patches. The middle metal layer is severed as the ground, and a fan-shaped bias line on the bottom metal layer is designed to reduce the influence of DC bias on RF performance. The three metal layers are all copper with a thickness of 0.035mm. The two dielectric layers are both Rogers RO4003C ($\varepsilon = 3.55$), and the upper layer's thickness is 1mm while that of the lower layer is 0.5mm. The PIN diode MACOM MADP-000907-14020 is selected due to its low insertion loss in the working frequency range. With different digital signals from digital control system applied to the PIN diode, the diode can be switched between "on" and "off" states. The topology of the digital control circuit is shown in the Appendix A. The equivalent circuit of the PIN diode in "on" and "off" states is shown in the left of Figure 2b, and the corresponding parameters are as follows: L = 0.05 nH, R_{on} = 4.2 Ω, R_{off} = 300 kΩ, C_{off} = 42 fF, according to the S-parameter file.
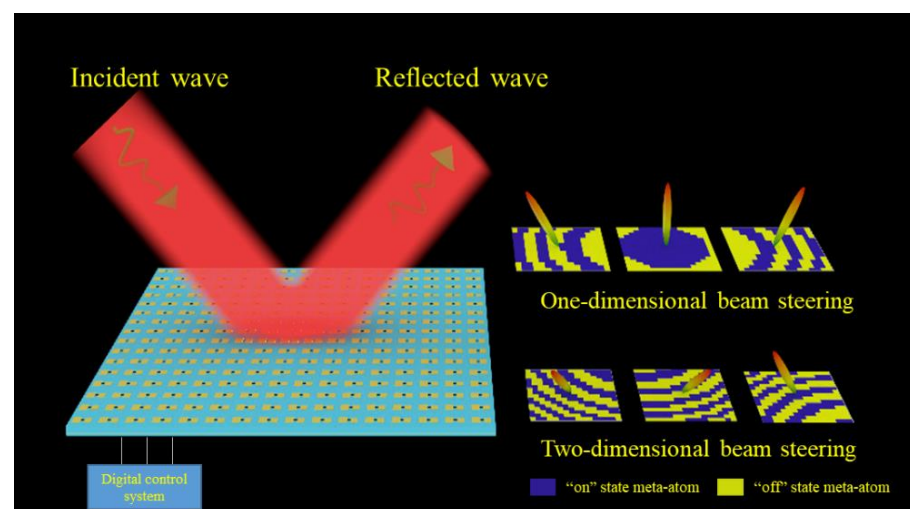

Figure 1. 3D schematic diagram of the proposed programmable coding metasurface with different beam manipulation functions. The digital control system provides the digital signals to control state of each meta-atom, and the beam and the corresponding coding pattern are shown in the right.
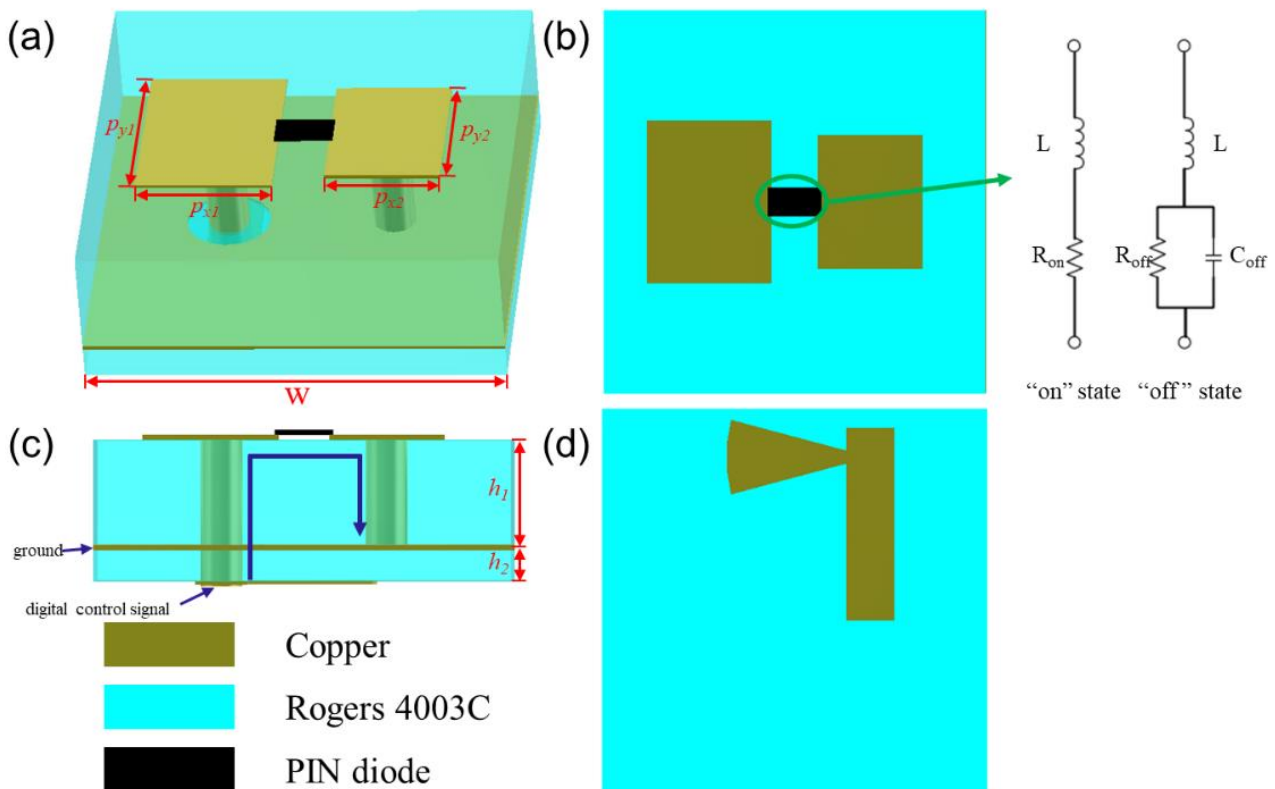
Figure 2. The 3D schematic diagram (**a**), top view (**b**), side view (**c**), and bottom view (**d**) of the meta-atom, where w = 4 mm, p_{x1} = 1.1 mm, p_{y1} = 1.4 mm, p_{x2} = 1.3 mm, p_{y2} = 1.7 mm, h_1 = 1 mm, h_2 = 0.5 mm. The left of (**b**) is the equivalent circuit of the PIN diode in "on" and "off" states. The blue arrows in (**c**) are the flow of the digital signal.

When a bias voltage is applied to the PIN diode, the diode switches between on and off depending on the voltage. When the meta-atom is irradiated with an x-polarized wave, the reflected wave will also be changed as the diode switches. The digital signal flows as shown by the blue arrows in Figure 2c: The left patch connects to the digital control board through a via hole, while the right patch connects to the ground through another via hole. The digital signal from the bottom metal passes through the left via hole to the left patch, flows to the right patch after the PIN diode, and finally connects to the ground by the right via hole. For the 1-bit metasurface, the phase difference of the two states should be optimized to 180°. The optimized structural parameters are as follows: w = 4 mm, p_{x1} = 1.1 mm, p_{y1} = 1.4 mm, p_{x2} = 1.3 mm, p_{y2} = 1.7 mm.

Figure 3 shows the simulated reflection amplitude and phase of the designed meta-atoms under an x-polarized incident wave, which is simulated by CST Microwave Studio software with a periodic boundary. When the PIN diode is switched from the "on" state to the "off" state, the phase of the reflected wave is changed from −66.4° to 112.7° at 27.75 GHz, which means the difference between the two states is 179.1°. In addition, the amplitude of the reflected wave is almost constant in the operating frequency band. The simulated results show that the proposed metasurface meta-atom satisfies the requirement of "0" and "1" meta-atoms for a 1-bit digital coding metasurface.
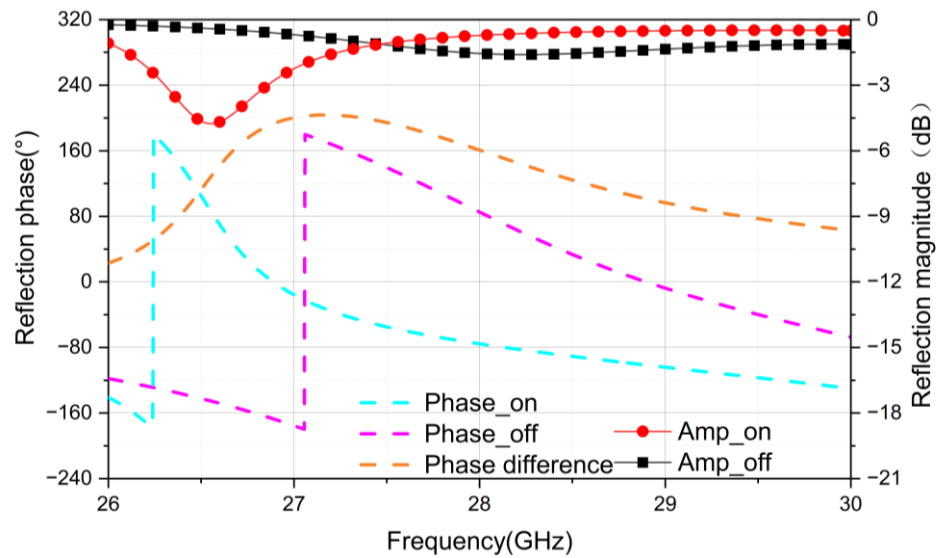
Figure 3. The simulated reflection amplitude and phase of the designed meta-atoms under x-polarized normal incident wave.

To verify the beam-modulating performance of the designed digital coding metasurface, we performed full-wave simulations of the metasurface with the radiation from a pyramidal horn antenna, which can emit a spherical wave. According to a generalized Snell's law of reflection, the direction of the reflected beam is determined by the phase gradient along the metasurface [4]:

$$\sin\theta_{\mathrm{r}} - \sin\theta_i = \frac{\lambda_0}{2\pi}\frac{d\varphi}{dx} \tag{1}$$

where θ_i is the angle of the incident wave, θ_r is the angle of the reflected wave, λ_0 is the wavelength, and $\frac{d\varphi}{dx}$ is the phase gradient. However, the wave excited by the horn is not a plane wave, and the phases of the impacted wave for these meta-atoms are different. Therefore, we can obtain the coordinates of the phase center of the transmitter horn through full-wave simulation, and the compensation phase for the meta-atom (m, n) can be written as:

$$\varphi_{\mathrm{c}}(m, n) = \frac{2\pi}{\lambda}\left|\vec{r}_{mn} - \vec{r}_f\right| \tag{2}$$

where $\vec{r}_{mn}$ and $\vec{r}_f$ are the position vectors of the meta-atom (m, n) and the phase center of the transmitter horn. Therefore, if the metasurface is normally incident by an EM wave $(\theta_{\mathrm{i}} = 0)$, the phase required for the meta-atom (m, n) can be written as [15]:

$$\varphi(m, n) = -\frac{2\pi}{\lambda_0}(md_x\sin\theta\cos\phi + nd_y\sin\theta\sin\phi) + \varphi_{\mathrm{c}}(m, n) + \varphi_0 \tag{3}$$

where θ and ϕ are the elevation and azimuth angles of the desired direction, d_x and d_y are the periodic lengths in the x and y directions, and φ_0 is the initial phase. The phase calculated by Equation (3) is a continuous value, so it needs to be quantized. The phase profile is calculated and quantized using the following equation:

$$code(m, n) = \begin{cases} 0 & 0 < \varphi(m, n) < \pi \\ 1 & \pi < \varphi(m, n) < 2\pi \end{cases} \tag{4}$$

Figure 4 is the simulated far-field of the beam steering in the xoz plane at 28 GHz, and the details of the simulated results are listed in Table 1, which is simulated by CST Microwave Studio software with a PML (perfectly matched layer) boundary. As can be seen, with the increase in deflection angle, the gain decreases and the half-power beam width

increases. The results are in good agreement with the designed ones, and the difference between the design angle and measured angle (beam-pointing error) is less than 3°. In addition, the specular reflection beam is significantly enhanced as the scan angle increases, which should be the reason for the decrease in gain. This problem is more pronounced when the beam scans to other directions in the upper half-plane, as shown in Figure 5.
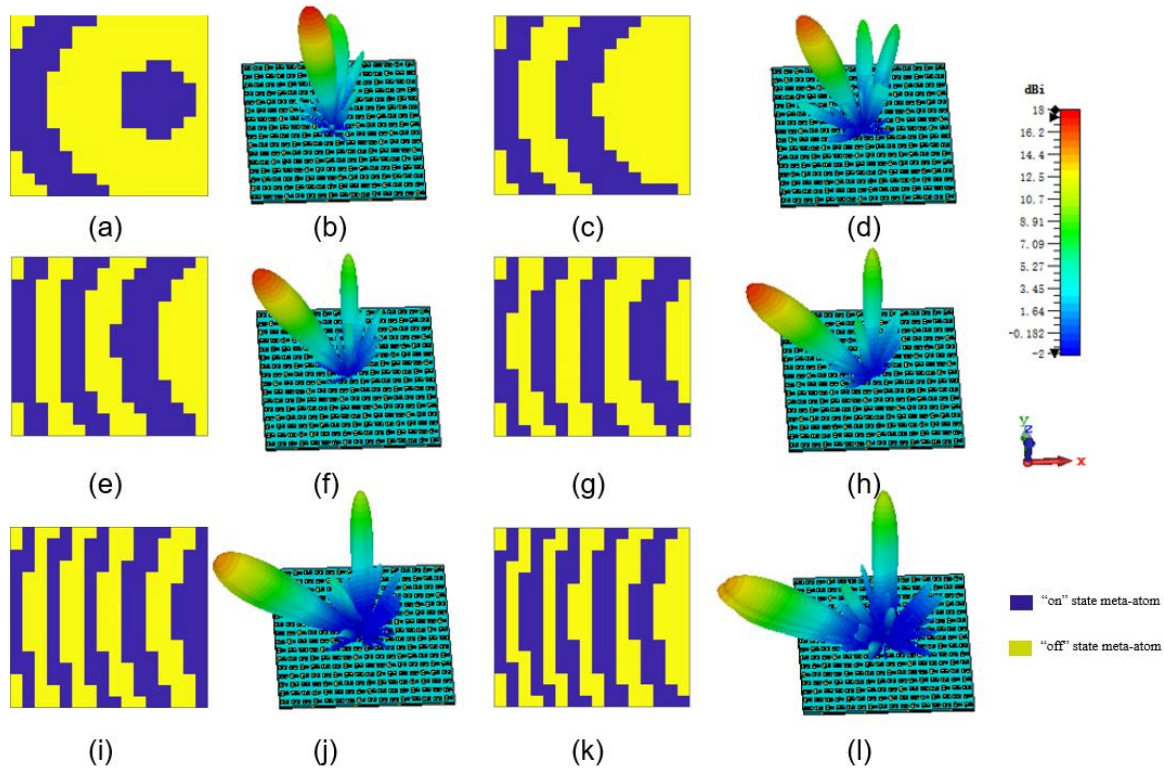

Figure 4. The coding pattern and simulated far−field pattern in the xoz plane. (**a**,**b**) 10°; (**c**,**d**) 20°; (**e**,**f**) 30°; (**g**,**h**) 40°; (**i**,**j**) 50°; (**k**,**l**) 60°. The simulations are under x−polarized normal incident wave.
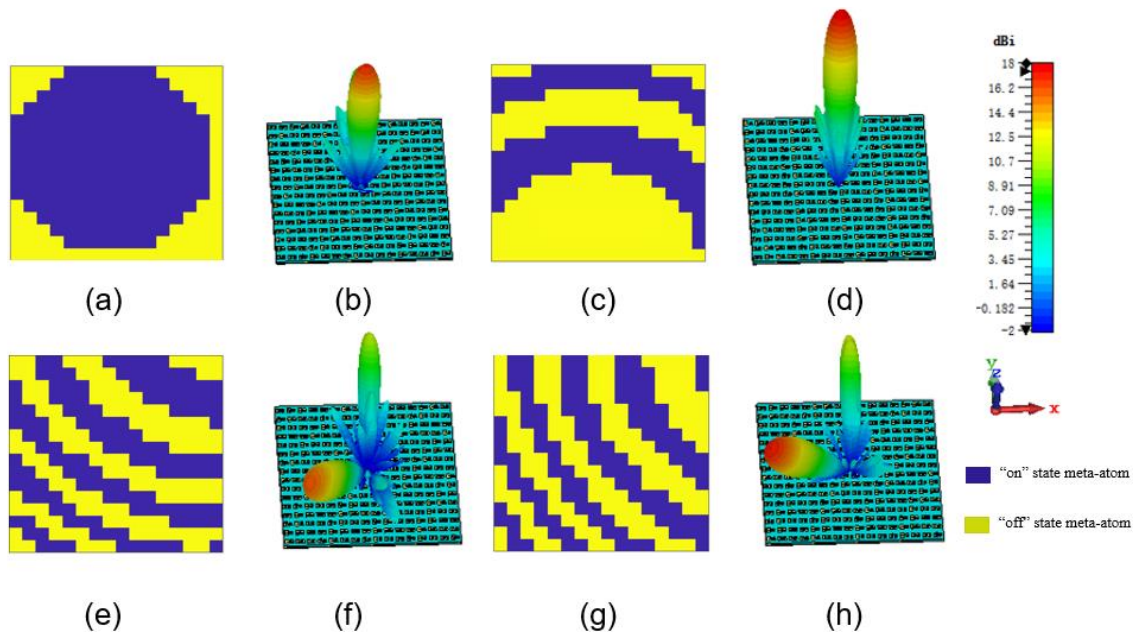
Figure 5. The coding pattern and simulated far−field pattern in other directions. (**a**,**b**) phi = 0°, theta = 0°; (**c**,**d**) phi = 90°, theta = 20°; (**e**,**f**) phi = 235°, theta = 40°; (**g**,**h**) phi = 210°, theta = 45°. The simulations are under x−polarized normal incident wave.

Table 1. Beam-steering performance at 28GHz.

Scan Angle	Gain (dBi)	Half-Power Beam Width	Beam-Pointing Error
10°	17.3	9.9°	−1°
20°	16.2	9.7°	0°
30°	16.8	10.7°	−1°
40°	17.0	11.6°	0°
50°	15.0	14.2°	−2°
60°	14.5	17.1°	0°

3. Experiments and Discussions

To verify the beam-steering capability of the proposed programmable metasurface, a prototype was fabricated using conventional printed circuit board (PCB) technology. The fabricated metasurface prototype is shown in Figure 6. The total size of the PCB is 6.6 mm × 12.2 mm, and size of the compact metasurface is 6.4 mm × 6.4 mm in the middle. The bias lines are connected to the designed control circuit board by a pin header.
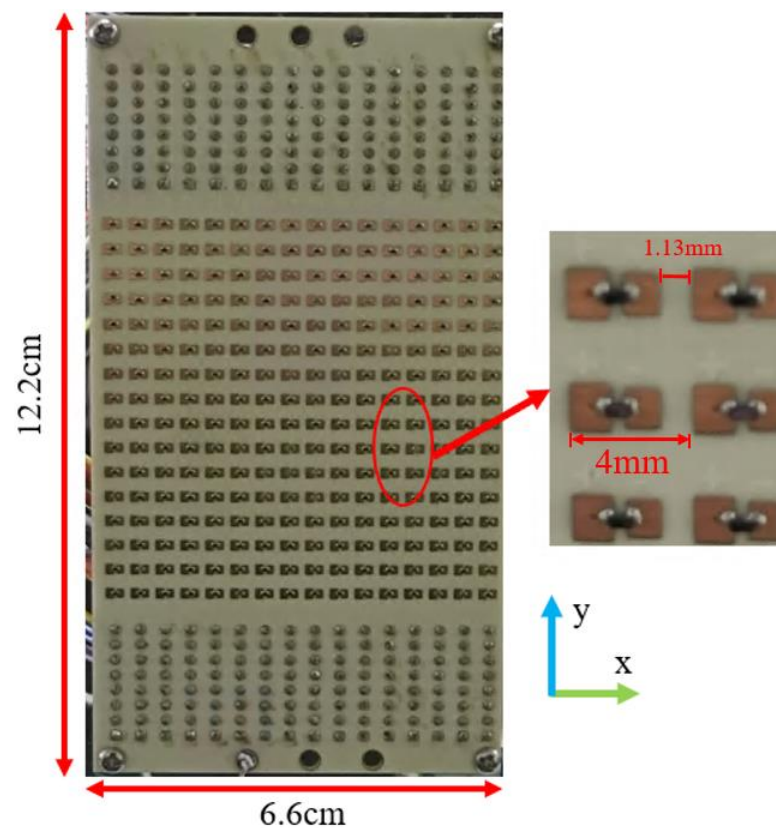
Figure 6. The photo of the prototype.

The beam deflection capability of the coding metasurface was measured in a standard anechoic chamber environment. As shown in Figure 7, the prototype was fixed at the center of the rotation stage. The transmitting horn antenna in front of the prototype was also fixed at the rotation stage, and the positions of the prototype and the transmitting antenna remained relatively fixed. In addition, the receiving horn was placed 3 m from the metasurface (see Appendix B). After applying the voltage that corresponded to different coding patterns, the EM wave with horizontal polarization was emitted by the horn antenna, deflected by the designed metasurface, and finally collected by the horn antenna at the receiving end, which was connected to the spectrum analyzer.
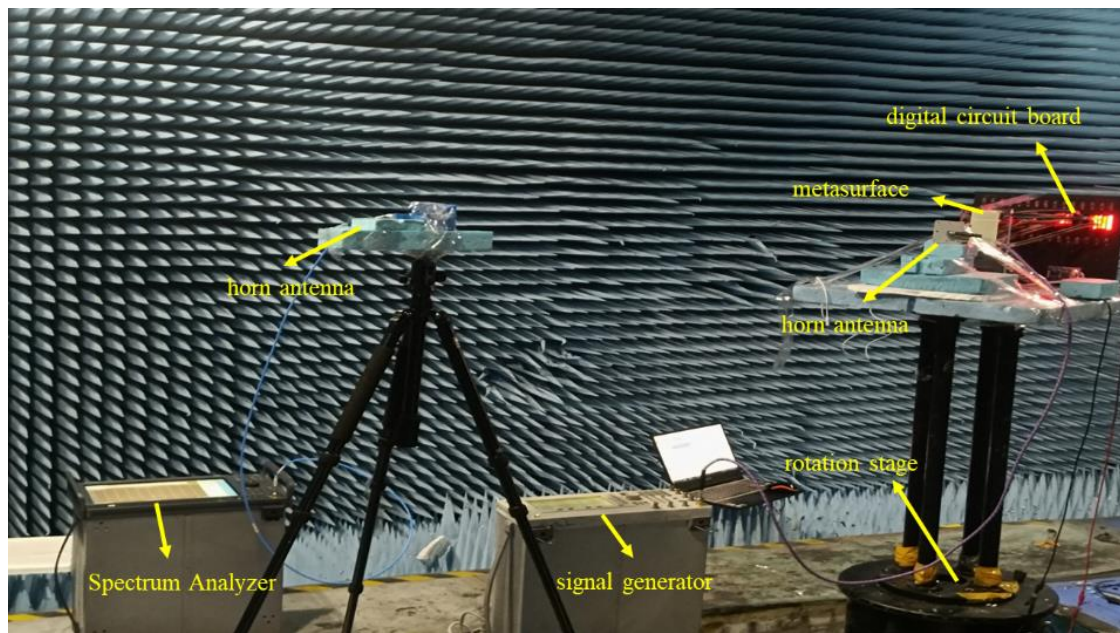
Figure 7. The Experimental setup for the characterization of the programmable metasurface performance.

The measured distribution of the reflected beam for different coding patterns in the xoz plane at 28 GHz is shown in Figure 8. Because of the block of the transmitting horn, the steering beam is slightly deformed when the deflection angle is less than 20°. With the increase in deflection angle, the gain of the metasurface decreases, and the half-power beam width increases, which is basically consistent with the design objective. Additionally, the left and right sides of the radiation patterns at some steering angles are not strictly symmetrical, which can be explained by the influence of the coaxial line on the reflected wave.
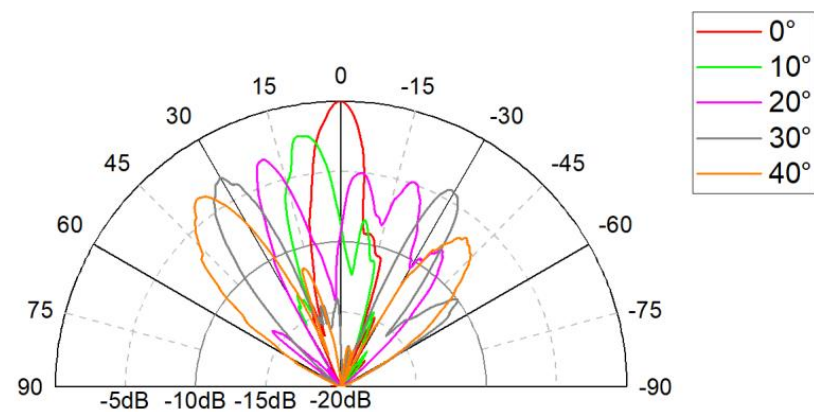

Figure 8. The measured results of beam steering at 28 GHz in the xoz plane. The measurements are under x−polarized incident wave.

To evaluate the broadband performance of the designed metasurface, the prototype was also measured at 29 GHz, and the results are demonstrated in Figure 9. The experimental far-field is close to the results at 28 GHz. Figure 10 shows the measured results of a 30° steering angle at three frequencies (28 GHz, 29 GHz, and 30 GHz). It can be seen that the gain and the direction of the beams remain in good consistency in the range of 28 GHz-30 GHz, while the side lobe level decreases with increasing frequency. The measured results confirm that the working frequency band of the metasurface can meet the design requirements.
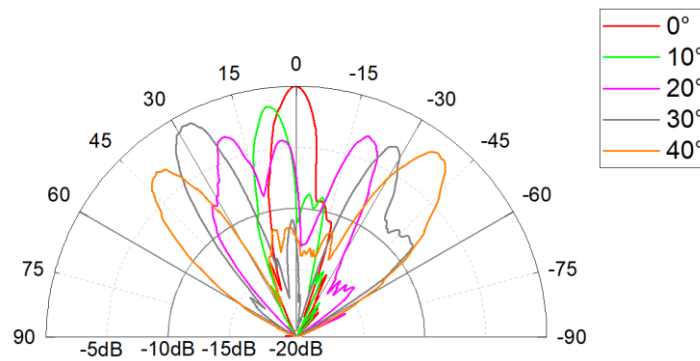
Figure 9. The measured results of beam steering at 29 GHz in the xoz plane. The measurements are under x−polarized incident wave.
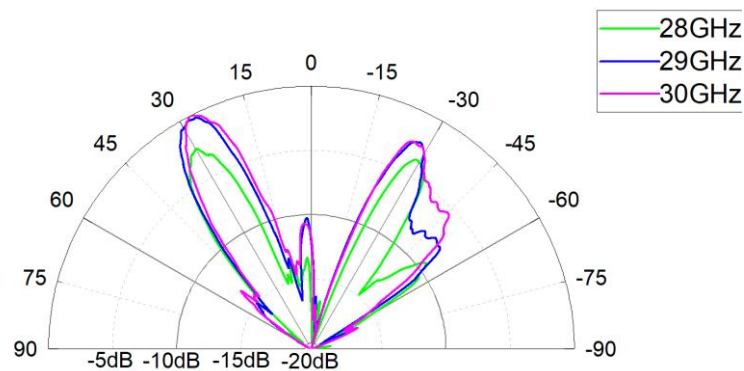

Figure 10. The measured results of 30° beam steering at three different frequencies. The measurements are under x−polarized incident wave.

The beam-steering ability in the yoz plane was also measured. Figure 11 indicates the measured results of beam steering at 28 GHz in the yoz plane. Compared to the performance in the xoz plane, the beams in the yoz plane are obviously worse. In addition to the effect of specular reflection, the fan-shaped bias line is placed in the y-direction, which may affect the steering performance of the metasurface's yoz plane. Moreover, the coupling of the atoms in the y-direction is strong, so the interference between adjacent meta-atoms further reduces the performance of the metasurface.
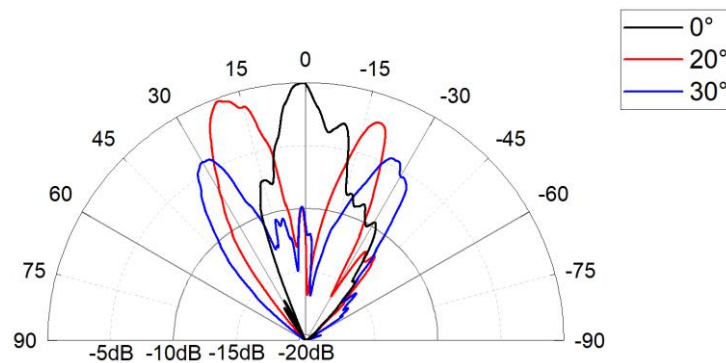

Figure 11. The measured results of beam steering at 28 GHz in the yoz plane. The measurements are under x−polarized incident wave.

4. Conclusions

In this paper, a 1-bit programmable metasurface is designed by loading PIN diodes. By switching the "on" and "off" states of the PIN diode, the meta-atoms can obtain a phase difference of 180° between the two states, and the return loss of the metasurface is better than −1.5 dB. The designed metasurface works in the Ka band, and each meta-

atom can be individually modulated by the digital circuit. With the phase compensation of the incident wave from the horn antenna, the metasurface realizes the beam steering by changing the phase distribution of the metasurface. Simulation results show that the metasurface can achieve flexible two-dimensional beam scanning in the upper half-plane with a maximum scanning angle of 60°. Experimental results show that the designed metasurface can achieve a maximum scan of 40° in the upper half-plane. The design offers a promising solution of beam steering at millimeter wave frequcncy. The designed programmable coding metasurfaces are expected to expand the potential applications for sensing and 5G wireless communications.

Institutional Review Board Statement: Not applicable.

Informed Consent Statement: Not applicable.

Data Availability Statement: Not applicable.

Conflicts of Interest: The authors declare no conflict of interest.

Appendix A

The topology of the digital control circuit is shown in the Figure A1. It is mainly composed of a FPGA and 32 8-bit shift registers. The shift register converts the serial signal into parallel signals, and each output signal is used to control one PIN diode on the metasurface.
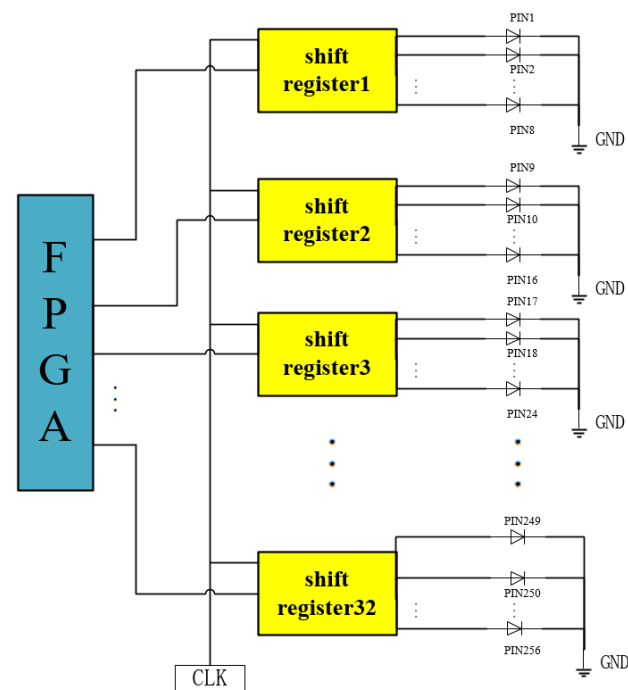

Figure A1. The topology of the digital control system.

Appendix B

The block diagram of the measurement is shown in the Figure A2. The prototype is fixed at the center of the rotation stage. The transmitting horn antenna in front of the prototype is also fixed at the rotation stage, and the positions of the prototype and the transmitting antenna remain relatively fixed. In addition, the receiving horn is placed 3 m from the metasurface.
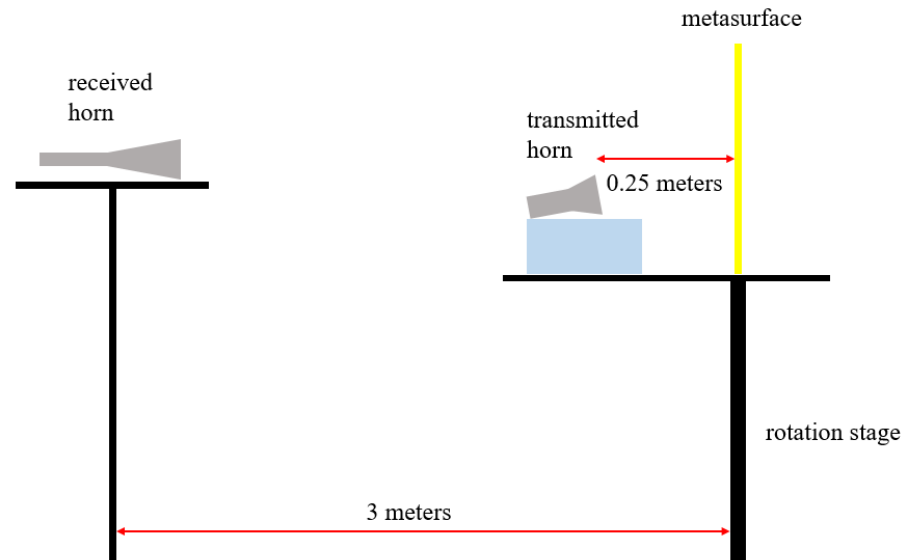

Figure A2. The block diagram of the measurement.

References

1. Zheludev, N.I.; Kivshar, Y.S. From Metamaterials to Metadevices. *Nat. Mater.* **2012**, *11*, 917–924. [CrossRef] [PubMed]
2. Li, C.; Yu, P.; Huang, Y.; Zhou, Q.; Wu, J.; Li, Z.; Tong, X.; Wen, Q.; Kuo, H.-C.; Wang, Z.M. Dielectric Metasurfaces: From Wavefront Shaping to Quantum Platforms. *Prog. Surf. Sci.* **2020**, *95*, 100584. [CrossRef]
3. Wang, J.; Li, Y.; Jiang, Z.H.; Shi, T.; Tang, M.-C.; Zhou, Z.; Chen, Z.N.; Qiu, C.-W. Metantenna: When Metasurface Meets Antenna Again. *IEEE Trans. Antennas Propagat.* **2020**, *68*, 1332–1347. [CrossRef]
4. Yu, N.; Genevet, P.; Kats, M.A.; Aieta, F.; Tetienne, J.-P.; Capasso, F.; Gaburro, Z. Light Propagation with Phase Discontinuities: Generalized Laws of Reflection and Refraction. *Science* **2011**, *334*, 333. [CrossRef] [PubMed]
5. Danila, O.; Manaila-Maximean, D. Bifunctional Metamaterials Using Spatial Phase Gradient Architectures: Generalized Reflection and Refraction Considerations. *Materials* **2021**, *14*, 2201. [CrossRef]
6. Danila, O. Polyvinylidene Fluoride-Based Metasurface for High-Quality Active Switching and Spectrum Shaping in the Terahertz G-Band. *Polymers* **2021**, *13*, 1860. [CrossRef] [PubMed]
7. Huang, C.X.; Zhang, J.; Cheng, Q.; Cui, T.J. Polarization Modulation for Wireless Communications Based on Metasurfaces. *Adv. Funct. Mater.* **2021**, *31*, 2103379. [CrossRef]
8. Wu, R.; Bao, L.; Wu, L.; Cui, T. Broadband Transmission-Type 1-Bit Coding Metasurface for Electromagnetic Beam Forming and Scanning. *Sci. China Phys. Mech. Astron.* **2020**, *63*, 284211. [CrossRef]
9. Zhang, Z.; Yan, X.; Liang, L.; Wei, D.; Wang, M.; Wang, Y.; Yao, J. The Novel Hybrid Metal-Graphene Metasurfaces for Broadband Focusing and Beam-Steering in Farfield at the Terahertz Frequencies. *Carbon* **2018**, *132*, 529–538. [CrossRef]
10. Wang, Z.X.; Wu, J.W.; Wu, L.W.; Gou, Y.; Ma, H.F.; Cheng, Q.; Cui, T.J. High Efficiency Polarization-Encoded Holograms with Ultrathin Bilayer Spin-Decoupled Information Metasurfaces. *Adv. Optical Mater.* **2020**, *9*, 2001609. [CrossRef]
11. Liu, C.; Yang, F.; Fu, X.; Wu, J.; Zhang, L. Programmable Manipulations of Terahertz Beams by Graphene-Based Metasurface With Both Amplitude and Phase Modulations. *Front. Mater.* **2022**, *9*, 932773. [CrossRef]
12. Zhang, L.; Chen, M.Z.; Tang, W.; Dai, J.Y.; Miao, L.; Zhou, X.Y.; Jin, S.; Cheng, Q.; Cui, T.J. A Wireless Communication Scheme Based on Space- and Frequency-Division Multiplexing Using Digital Metasurfaces. *Nat. Electron.* **2021**, *4*, 218–227. [CrossRef]
13. Pedross-Engel, A.; Watts, C.M.; Smith, D.R.; Reynolds, M.S. Enhanced Resolution Stripmap Mode Using Dynamic Metasurface Antennas. *IEEE Trans. Geosci. Remote Sens.* **2017**, *55*, 3764–3772. [CrossRef]
14. Yang, H.; Yang, F.; Xu, S.; Mao, Y.; Li, M.; Cao, X.; Gao, J. A 1-Bit 10×10 Reconfigurable Reflectarray Antenna: Design, Optimization, and Experiment. *IEEE Trans. Antennas Propagat.* **2016**, *64*, 2246–2254. [CrossRef]
15. Cui, T.J.; Qi, M.Q.; Wan, X.; Zhao, J.; Cheng, Q. Coding Metamaterials, Digital Metamaterials and Programmable Metamaterials. *Light Sci. Appl.* **2014**, *3*, e218. [CrossRef]
16. Cui, T.J.; Li, L.; Liu, S.; Ma, Q.; Zhang, L.; Wan, X.; Jiang, W.X.; Cheng, Q. Information Metamaterial Systems. *iScience* **2020**, *23*, 101403. [CrossRef] [PubMed]

17. Zhang, X.G.; Tang, W.X.; Jiang, W.X.; Bai, G.D.; Tang, J.; Bai, L.; Qiu, C.-W.; Cui, T.J. Light-Controllable Digital Coding Metasurfaces. *Adv. Sci.* **2018**, *5*, 1801028. [CrossRef] [PubMed]

18. Zhang, L.; Chen, X.Q.; Liu, S.; Zhang, Q.; Zhao, J.; Dai, J.Y.; Bai, G.D.; Wan, X.; Cheng, Q.; Castaldi, G.; et al. Space-Time-Coding Digital Metasurfaces. *Nat. Commun.* **2018**, *9*, 4334. [CrossRef]

19. Dai, J.Y.; Tang, W.; Yang, L.X.; Li, X.; Chen, M.Z.; Ke, J.C.; Cheng, Q.; Jin, S.; Cui, T.J. Realization of Multi-Modulation Schemes for Wireless Communication by Time-Domain Digital Coding Metasurface. *IEEE Trans. Antennas Propagat.* **2020**, *68*, 1618–1627. [CrossRef]

20. Liu, C.X.; Yang, F.; Fu, X.J.; Wu, J.W.; Zhang, L.; Yang, J.; Cui, T.J. Programmable Manipulations of Terahertz Beams by Transmissive Digital Coding Metasurfaces Based on Liquid Crystals. *Adv. Optical Mater.* **2021**, *4*, 1470–1474. [CrossRef]

21. Yang, J.; Zhang, C.; Ma, H.; Yuan, W.; Yang, L.; Ke, J.; Chen, M.; Mahmoud, A.; Cheng, Q.; Cui, T. Tailoring Polarization States of Multiple Beams That Carry Different Topological Charges of Orbital Angular Momentums. *Opt. Express* **2018**, *26*, 31664. [CrossRef] [PubMed]